CALPHAD: Computer Coupling of Phase Diagrams and Thermochemistry 34 (2010) 20–25

Contents lists available at ScienceDirect

CALPHAD: Computer Coupling of Phase Diagrams and Thermochemistry

journal homepage: www.elsevier.com/locate/calphad

Solvus boundaries of (meta)stable phases in the Al–Mg–Si system: First-principles phonon calculations and thermodynamic modeling

H. Zhang [a,*], Y. Wang [a], S.L. Shang [a], C. Ravi [b], C. Wolverton [c], L.Q. Chen [a], Z.K. Liu [a]

[a] Department of Materials Science and Engineering, The Pennsylvania State University, 304 Steidle Building, University Park, PA 16802, USA

[b] Materials Science Division, Indira Gandhi Centre for Atomic Research, Kalpakkam 603 102, India

[c] Department of Materials Science and Engineering, Northwestern University, 2220 Campus Drive, Evanston, IL 60208-3108, USA

ARTICLE INFO

Article history:
Received 12 June 2009
Received in revised form
25 October 2009
Accepted 26 October 2009
Available online 10 November 2009

Keywords:
First-principles calculations
Intermetallic compounds
Metastable phases
CALPHAD

ABSTRACT

Using first-principles total energies and frozen phonon calculations, we predict the thermodynamic properties (enthalpies of formation and vibrational entropies) for three phases in the Al–Mg–Si system: the stable phase (β-Mg_2Si), and two metastable precipitate phases (β'-$Mg_{18}Si_{10}$ and β''-Mg_5Si_6). The stable fcc/β and the metastable fcc/β' and fcc/β'' phase boundaries are obtained from a combination of the Gibbs energy of the compounds determined from first-principles and the free energy of the Al-rich solid solution (fcc phase) taken from the literature. Predicted phase boundaries show good agreement with available phase stability measurements. The present work demonstrates the capability of first-principles calculations in predicting Gibbs energies of stable and metastable phases.

1. Introduction

Alloys based on the Al–Mg–Si system are widely used for engineering applications due to their excellent mechanical properties. In particular, the strength of Al–Mg–Si alloys can be significantly increased through age hardening, during which various metastable phases form. Although there are a wealth of metastable phases observed in these alloys, the generic precipitate formation sequence in Al–Mg–Si alloys is the following [1–3]:

$$\text{Atomic clusters} \rightarrow \text{Guinier–Preston (GP) zones} \rightarrow \beta'' \rightarrow \beta' \rightarrow \beta,$$

where β'', β' and β represent the metastable Mg_5Si_6 and $Mg_{18}Si_{10}$ and the stable Mg_2Si compounds, respectively. The GP zones consist of distinctive clusters with compositions different from the overall alloy composition [4]. The needle-shaped β'' phase is often considered the most effective hardening precipitate [2,5], while the formation of the rod-shaped precipitate β' phase can indicate that the alloy is over-aged [6].

Despite nearly one hundred years of study of this important system, accurate positions of the metastable phase boundaries which are needed for quantitative simulation of the aging process are not known. These phase boundaries are very difficult to determine reliably from experiments due to the transient nature of metastable phases. In the present work, first-principles density-functional theory calculations [7,8] are performed in an effort to obtain the key thermodynamic properties necessary to quantitatively predict the thermodynamic limit of these metastable boundaries. From static total energy calculations, we obtain the equilibrium structural properties of Mg, Si, β, β' and β'' and the enthalpies of formation of β, β' and β''. Using frozen-phonon calculations, we also ascertain the vibrational entropies of formation for each phase. This combination of first-principles calculated enthalpies and entropies for stable and metastable phases allows us to compare trends in the enthalpy vs. entropy for β, β' and β'', as well as these thermodynamic functions with the observed precipitation sequence given above. Combining this first-principles thermodynamic information together with the Gibbs energy of the Al-rich solid solution containing Si and Mg (fcc phase) from the CALPHAD approach [9], we predict the stable and metastable phase boundaries for fcc/β, fcc/β' and fcc/β''. Our work is guided by previous studies of the first-principle prediction of solvus boundaries in Al alloys. In particular, the solvus boundaries for stable phases in binary systems were investigated, e.g. Al–Sc [10] and Al–Si [11]. Subsequently, this work was extended to include both stable and metastable phase boundaries in Al–Cu [12]. In the present work, we extend these previous studies by predicting solvus boundaries in the Al–Mg–Si ternary system, including both stable and metastable precipitate phases. In addition, our work explores the approach of combining first-principles calculated thermodynamic functions of the (meta)stable

* Corresponding author. Tel.: +1 814 8639957.
E-mail address: huz106@psu.edu (H. Zhang).

0364-5916/$ – see front matter © 2009 Elsevier Ltd. All rights reserved.
doi:10.1016/j.calphad.2009.10.009

Table 1
Calculated and experimental lattice parameters (Å) and Debye temperature Θ_D (K).

Phase	Space group	Lattice parameter (Å)						Θ_D (K)	
		This work			Exp.			This work	Exp.
		a	*b*	*c*	*a*	*b*	*c*		
Mg	$P6_3/mmc$	3.21		5.11	3.21 [49]		5.21 [49]	316	330 [20]
Si	$Fd\bar{3}m$	5.45			5.43 [21]			649	645 [22]
β-Mg_2Si	$Fm\bar{3}m$	6.37			6.35 [18]			416	417 [23]
β'-$Mg_{18}Si_{10}$	$P6_3$	7.15		4.14	7.15 [17,18,24]		4.05 [17,18,24]	399	N/A
β''-Mg_5Si_6	$C2/m$	14.24	4.07	6.98	15.16 [15,16]	4.05 [15,16]	6.74 [15,16]	398	N/A

intermetallic phases with CALPHAD data for the solid solution, in order to achieve more quantitatively accurate phase boundaries.

2. Method

In the present work, the first-principles calculations are performed by employing the Vienna *ab initio* simulation package (VASP) [7,8] with Vanderbilt ultrasoft pseudopotentials [13] and the generalized gradient approximation (GGA) [14]. The crystal structure data of β-Mg_2Si, β'-$Mg_{18}Si_{10}$, and β''-Mg_5Si_6 are summarized in Table 1 [15–18] with β having the cubic CaF_2 structure [4], β' hexagonal and β'' monoclinic structures [2,5], respectively. We use an energy cutoff of 188.3 eV, i.e., 1.25 times of the energy cutoff of Si, higher than those of Al and Mg, suggested by VASP. All calculations are performed with a complete relaxation of cell volume, cell vectors and cell-internal atomic positions. The Monkhorst–Pack scheme is used for the Brillouin-zone integrations [19]. The settings of k-points correspond roughly to an 8000 k-point mesh per reciprocal-atom.

In this study, the Helmholtz free energies for Mg, Si, β, β' and β'', are described by the harmonic approximation at the equilibrium volume [25–27],

$$F(T) = E_0 + F_{ph}(T), \tag{1}$$

where E_0 is the first-principles ground state energy at 0 K, and $F_{ph}(T)$ [25–27] the phonon contributions to the free energy. Since we are focused on the difference of thermodynamic properties (e.g. enthalpy of formation, entropy of formation) for compounds compared with the pure elements. It is worth mentioning that the anharmonic effects can be neglected here. From the phonon density of states, the lattice vibrational free energy can be calculated through [25–27]:

$$F_{ph}(T) = k_B T \int \ln\left\{2\sinh\left[\frac{h\nu}{2k_B T}\right]\right\} g(\nu)\mathrm{d}\nu, \tag{2}$$

where T is the temperature, k_B the Boltzmann constant, h the Planck constant, and $g(\nu)$ the phonon density of states as a function of phonon frequency ν. At zero pressure, the internal energy and Helmholtz free energy are equal to the enthalpy and Gibbs energy, respectively.

The vibrational properties of the structures can alternatively be characterized by their Debye temperatures Θ_D, which can be calculated by [28,29]:

$$k_B\Theta_D = h\nu_D(n) \tag{3}$$

$$\nu_D(n) = \left[\frac{n+3}{3}\int_0^\infty \nu^n g(\nu)\mathrm{d}\nu\right]^{1/n} \quad (n \neq 0, n > -3), \tag{4}$$

where $\nu_D(n)$ is the Debye cutoff frequency. The cutoff frequency for $n = -2$ is used in this work, and hence the integrals in Eqs. (3) and (4) can get $\Theta_D(-2)$. $\Theta_D(-2)$ has an important physical meaning as it is related to the root-mean-square amplitude of thermal oscillations according to the Debye–Waller theory [30,31].

The phonon density of states ($g(\nu)$ in Eq. (2)) for hcp–Mg, diamond–Si, β-Mg_2Si, β'-$Mg_{18}Si_{10}$ and β''-Mg_5Si_6 are calculated using the supercell method implemented in the ATAT package [32] as the interface to the VASP code [7,8]. The supercell method is based on the frozen phonon approximation through which the changes in total energy and forces are calculated in the direct space by displacing the atoms from their equilibrium positions. The main steps for the first-principles phonon calculation in ATAT are: (i) Assign the primitive unit cell and fully relax the primitive unit cell by first-principles code (VASP in this work). (ii) Select the size of the supercell according to the defined neighbor interaction distance, making perturbation to the atomic positions, and calling the first-principles code to calculate the forces imposed on the atoms. (iii) Fit the force constants from the forces and calculate the phonon frequencies with the assigned cutoff range for force constants. The supercell sizes N in the phonon calculations for Mg, Si, β-Mg_2Si, β'-$Mg_{18}Si_{10}$ and β''-Mg_5Si_6 contained 52, 96, 96, 84, and 88 atoms, respectively. The number of k points, N_k, is determined through $N \times N_k = 4000$.

The enthalpy of formation of a compound is defined as the difference in total energy of the compound and the energies of its constituent elements in their stable states:

$$\Delta_f H(\mathrm{Mg}_x\mathrm{Si}_y) = E(\mathrm{Mg}_x\mathrm{Si}_y) - \frac{x}{x+y}E(\mathrm{Mg}) - \frac{y}{x+y}E(\mathrm{Si}) \tag{5}$$

where $E(\mathrm{Mg}_x\mathrm{Si}_y)$, $E(\mathrm{Mg})$ and $E(\mathrm{Si})$ are the energies of the compound $\mathrm{Mg}_x\mathrm{Si}_y$ and constituents, hcp–Mg and diamond–Si, respectively.

To calculate the phase boundaries, the Gibbs energy of the fcc solution phase is taken from the work by Feufel et al. [9] shown in Table 2. Ideally, one would use the free energy of fcc also from the first-principles calculations. Indeed, in a recent study [33], the enthalpy of mixing in the ternary fcc Al–Mg–Si phase was calculated, showing the discrepancies with the data in the literature for the binary and the ternary systems. The present work focuses on developing an approach to insert the metastable phases into multi-component Al and Mg thermodynamic databases and demonstrating its feasibility. The enthalpies and entropies of formation of β, β' and β'' are obtained from first-principles calculations in the present work. The Gibbs energy of compounds can be described as:

$$G^{\mathrm{Mg}_a\mathrm{Si}_b} = a\,{}^0G^{\mathrm{hcp}}_{\mathrm{Mg}} + b\,{}^0G^{\mathrm{diamond}}_{\mathrm{Si}} + \Delta_f H^{\mathrm{Mg}_a\mathrm{Si}_b} - T\Delta_f S^{\mathrm{Mg}_a\mathrm{Si}_b} \tag{6}$$

where ${}^0G^{\mathrm{hcp}}_{\mathrm{Mg}}$ and ${}^0G^{\mathrm{diamond}}_{\mathrm{Si}}$ are the molar Gibbs energies of the pure element hcp Mg and diamond Si, from the widely accepted Scientific Group Thermodata Europe (SGTE) data [34], respectively. The Gibbs energy of formation of the compound can be written as: $\Delta_f H^{\mathrm{Mg}_a\mathrm{Si}_b} - T\Delta_f S^{\mathrm{Mg}_a\mathrm{Si}_b}$, where $\Delta_f H^{\mathrm{Mg}_a\mathrm{Si}_b}$ and $\Delta_f S^{\mathrm{Mg}_a\mathrm{Si}_b}$ are the enthalpy and entropy of formation calculated from first-principles.

3. Results and discussion

3.1. First-principles results

In this section, the calculated equilibrium lattice parameters, phonon density of states, together with the predicted finite

Table 2
Thermodynamic parameters of fcc phase in the Al–Mg–Si system, in SI unit. fcc description: $G_m^{fcc} = \sum x_i {}^0G_i^{fcc} + RT\sum x_i \ln x_i + \sum_i \sum_{j>i} x_i x_j \sum_{k=0}^{n} {}^kL_{i,j}^{fcc}(x_i - x_j)^k$.

Parameters
${}^0L_{Al,Mg}^{fcc} = 4971 - 3.5T$
${}^1L_{Al,Mg}^{fcc} = 900 + 0.423T$
${}^2L_{Al,Mg}^{fcc} = 950$
${}^0L_{Al,Si}^{fcc} = -3143.78 + 0.29397T$
${}^0L_{Mg,Si}^{fcc} = -7148.79 + 0.89361T$

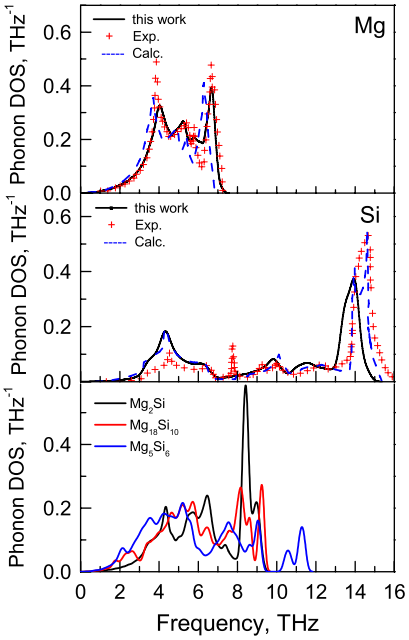

Fig. 1. Phonon density of states for Mg, Si, β-Mg_2Si, β'-$Mg_{18}Si_{10}$ and β''-Mg_5Si_6 phases in comparison with the available experimental data [35,36] and previous calculations [37,21].

temperature thermodynamic properties (entropy, enthalpy, and Gibbs energy) are presented and compared with the available experimental data.

Table 1 gives the predicted lattice parameters of hcp–Mg, diamond–Si, β-Mg_2Si, β'-$Mg_{18}Si_{10}$ and β''-Mg_5Si_6 at 0 K, which are in good agreement with the experimental data at room temperature. The phonon density of states (DOS) of Mg, Si, β-Mg_2Si, β'-$Mg_{18}Si_{10}$ and β''-Mg_5Si_6 calculated at the equilibrium volumes are plotted in Fig. 1. The available Raman measurements [35,36] and the previous calculations [37,21] of Mg and Si are included for comparison, showing good agreement. The predicted frequency of Si is slightly lower than the measured ones due to a weak bonding of Si predicted by the present calculations. The calculated lattice parameter of 5.45 Å is slightly larger than the measured lattice parameter 5.43 Å [38] (see Table 1). The peak with frequency around 7.8 THz can not be reproduced in the present work, which has been previously noted as a disagreement between first-principles calculations and experimental phonon DOS [21,20].

Comparing the phonon density of states of β-Mg_2Si, β'-$Mg_{18}Si_{10}$ and β''-Mg_5Si_6 as shown in Fig. 1(c), the distributions of vibrational frequencies in the lower frequency region (e.g, less than 5 THz) increase from Si, β, β', β'', to Mg, indicating the increase of phonon contributions to Gibbs energies from Si, β, β', β'', to Mg (cf. Eq. (2) and Fig. 3). In principle, the higher value of the phonon density of states in the lower frequency region implies a weak bonding nature and correspondingly a lower Debye temperature [27]. In terms of the second-moment Debye cutoff frequencies calculated from phonon density of states in Fig. 1, Table 1 summarizes the

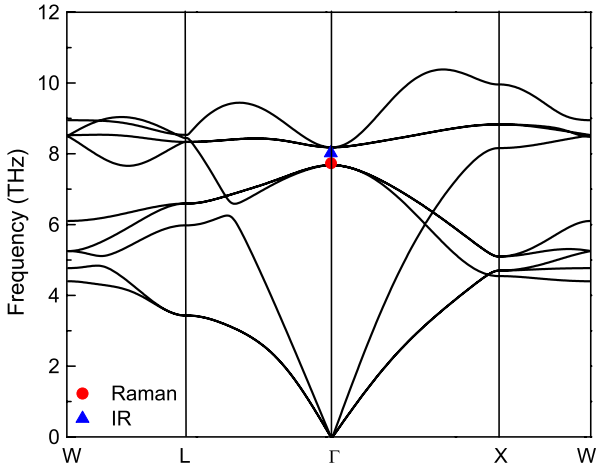

Fig. 2. Calculated phonon dispersion curves of β-Mg_2Si pertaining to the equilibrium volume at 0 K, and experimental frequencies [40,41] at the point are compared. Note that the LO/TO splitting is not calculated for the infrared active mode.

predicted Debye temperatures, which agree well with the available measurements [22,23,39]. It is shown that the Debye temperatures decrease from Si, β, β', β'', to Mg, which is consistent with the distributions of phonon density of states in the lower frequency region. The increase of Debye temperatures from β'', β', to β confirms again the strengthened bonds from β'', β', to β.

In order to validate the first-principles phonon calculations, one of the most important steps is to calculate the phonon dispersion. To our knowledge, there is no experimental phonon data of, β' and β'', except for the measured Γ point data of β-Mg_2Si. Fig. 2 shows the calculated phonon dispersion for β-Mg_2Si pertaining to the equilibrium volume at 0 K, which are in good agreements with the available Raman [40] and infrared measurements measured at room temperature [41]. As Mg_2Si is known to be a small band gap semiconductor, we should note that the Coulomb interactions will cause the frequencies of longitudinal optical (LO) modes above those of transversal optical (TO) modes [42,24,43]. The LO/TO splitting occurs at the Γ point of the Brillouin zone, and only for infrared active modes. However, the supercell method used in the present work cannot be employed to estimate the LO/TO splitting directly. It also should be mentioned that the LO modes contribute very little to the phonon DOS's, because they differ from TO modes only in a small volume of the reciprocal lattice in the vicinity of the Γ point [44]. Therefore, the present work does not take into account the influences of LO/TO splitting.

From the harmonic approximation, Fig. 3 shows the phonon contribution to enthalpies, entropies and Gibbs energies of Mg, Si, β-Mg_2Si, β'-$Mg_{18}Si_{10}$ and β''-Mg_5Si_6, where the total energy at 0 K is excluded. Note the diverse values of enthalpy at 0 K indicating the zero-point vibrational energies for each phase are different, whereas with an increasing temperature, the vibrational contributions to enthalpy approach to classical limit of 3RT regardless of different materials. Only small differences of enthalpy exist among β-Mg_2Si, β'-$Mg_{18}Si_{10}$ and β''-Mg_5Si_6, while there are more significant differences among the calculated vibrational entropies. The entropy of β'' increases with temperature more quickly than those of β and β' phases. Consequently, the Gibbs energy of β''-Mg_5Si_6 decreases faster than those of β-Mg_2Si and β'-$Mg_{18}Si_{10}$ at high temperatures.

The predicted room temperature (298 K) entropies and enthalpies of formation of β, β', and β'' phases are listed in Table 3. These quantities are calculated from a combination of the total energy at 0 K and thermodynamic phonon contributions. The enthalpies of formation calculated at 298 K decrease in the same order as the observed precipitation sequence: $\Delta H(\beta''\text{-}Mg_5Si_6)$ >

Table 3
Enthalpy and entropy of formation, $\Delta_f H$ (kJ/mol-atom) and $\Delta_f S$ (J/K mol-atom), at 298 K, respectively.

Phase	$\Delta_f H$	Method	$\Delta_f S$	Method
β''-Mg_5Si_6	3.5	This work	4.5	This work
	3.3	First-principles [45]		
β'-$Mg_{18}Si_{10}$	−12.6	This work	0.2	This work
	−11.7	First-principles [45]		
β-Mg_2Si	−17.7	This work	−1.8	This work
	−21.74	CALPHAD [9]	−2.68	CALPHAD [9]
	−18.0	First-principles [45]	−9.0	Vapor pressure [53]
	−26.3	Calorimetry [54]	−9.3	EMF [55]
	−14.21	Vapor pressure [53]	−2.68	Via heat capacity [47]
	−26.37	Calorimetry [56]	−5.37	Via heat capacity [57]
	−26.67	EMF [55]	−6.81	Via heat capacity [58]
	−22.99	Vapor pressure [46]	−4.72	EMF [48]
	−22.16	EMF [48]		
	−21.10	Calorimetry [9]		

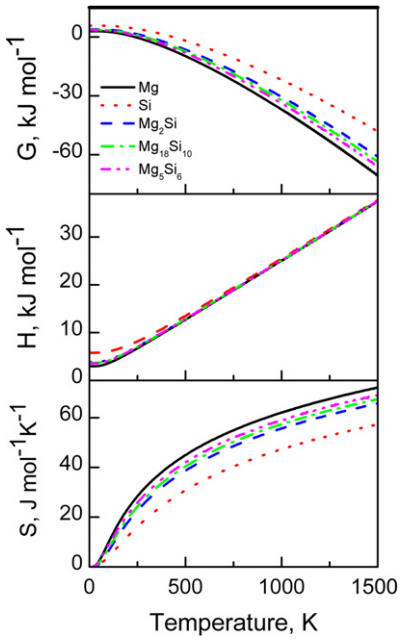

Fig. 3. Vibrational contributions to entropy (S), enthalpy (H), and Gibbs energy (G) for Mg, Si, β-Mg_2Si, β'-$Mg_{18}Si_{10}$ and β''-Mg_5Si_6 phases, in per mole of atom.

$\Delta H(\beta'\text{-}Mg_{18}Si_{10}) > \Delta H(\beta\text{-}Mg_2Si)$. The first-principles calculations show a correlation between decreasing energy and increasing Mg:Si ratio as the precipitation process proceeds, consistent with previous first-principles calculations by Ravi and Wolverton [45]. Table 3 also includes a comparison between the experimental enthalpies of formation of β-Mg_2Si, prior first-principles calculations [45], and the COST507 database [9]. The experimental values of the enthalpy of formation of Mg_2Si scatter over a large range. In view of the large difference in the melting points of Mg and Si as well as the large differences of their vapor pressures and densities, preparation of Mg–Si alloys can be extremely difficult. On the other hand, in the isopiestic technique, the Mg–Si alloy is obtained directly from a vapor pressure experiment taking advantage of the large difference in vapor pressures of the elements. Therefore, among all the techniques, we suggest that the isopiestic technique employed by Eldridge et al. [46] is more suited for this system compared with the other vapor pressure measurements as suggested by Geffken and Miller [47]. More recently, the value of the enthalpy of formation of Mg_2Si determined by Feufel et al. [9] is -21.12 ± 2.54 kJ/mole-atom. Values of the standard enthalpy of formation of Mg_2Si determined by Eldridge et al. [46], Rao et al. [48], and Feufel et al. [9] from vapor pressure, EMF, and calorimetric methods are in accord with each other. The first-principles calculated enthalpy of formation for β-Mg_2Si at 298 K is about 19% (4 kJ/mole-atom) less negative than these values. We also compare our results with those of Ravi and Wolverton [45] who have recently reported enthalpies of formation of β''-Mg_5Si_6, β'-Mg_2Si and β-Mg_2Si precipitates from first-principles. We see in Table 3 that the enthalpy of formation of β' in [45] is slightly less negative than the present value. It should be noted that the present work used the crystal structure of β' proposed by Andersen et al. [49] while the prior work [45] assumed a different crystal structure with composition $Mg_{1.8}Si$. The enthalpies of formation are listed in Table 3. We note that the crystal structure of β' proposed by Andersen et al. [49] yields a lower total energy in the DFT calculations. The calculated values of lattice parameters for β' phase are also in good agreement with the measurements, as shown in Table 1. We assert that the crystal structure and composition of β' proposed by Andersen et al. [49] is supported by our first-principle calculations. Table 3 also gives the calculated vibrational entropies of formation for stable and metastable phases. It can be seen that the entropies of formation calculated at 298 K decrease in the same order as the enthalpies of formation: $S(\beta''\text{-}Mg_5Si_6) > \Delta S(\beta'\text{-}Mg_{18}Si_{10}) > \Delta S(\beta\text{-}Mg_2Si)$. The stable phase has the lowest entropy of formation. This correlation between entropies and enthalpies of formation has also previously been found in DFT studies the Al–Cu system [12]. Due to the fact that the standard entropy determined from integration of the low temperature heat capacities can have significant uncertainty [47], we consider the very small magnitude of our calculated entropy of formation of β-Mg_2Si −1.8J/K mol-atom to be in reasonably good agreement with the COST507 database value of −2.68J/K mol-atom, based on the experiment by Geffken and Miller [47].

3.2. Phase diagram of Al solvus

In this section, we use our DFT calculated thermodynamic properties to calculate the (meta)stable phase stabilities of β'', β' and β phases. The Gibbs energy function of the fcc phase is taken from Feufel et al. [9] and is shown in Table 2. For the stable β-Mg_2Si and metastable β' and β'' phases, the enthalpies and entropies of formation are calculated from first-principles.

The calculated phase boundaries of fcc/β are shown in the vertical section from Al to Mg_2Si in Fig. 4, compared with experimental data and those calculated from the COST507 database. We note that there is considerable scatter in the reported experimental data for the ternary solubility of the stable β-Mg_2Si phase in an Al solid solution. Due to the fact that the starting materials contained relatively high impurities, e.g. 99.98 wt.% Mg and 98.64 wt.% Si [50]; 97.90 wt.% Mg and 99.48 wt.% Si [51] and the fact that the investigation was done with a very low concentration

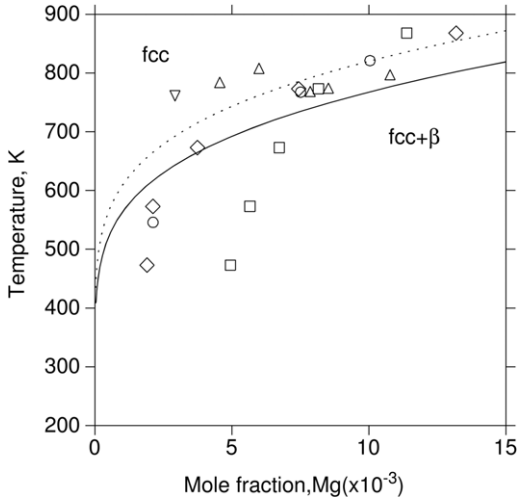

Fig. 4. Calculated solvus boundaries in the isopleth from Al to Mg_2Si in the present work (solid line) in comparison with COST507 database [9] (dotted line) and literature data (○ △ □ ◊ ▽) fcc − β solidus [9,50–52].

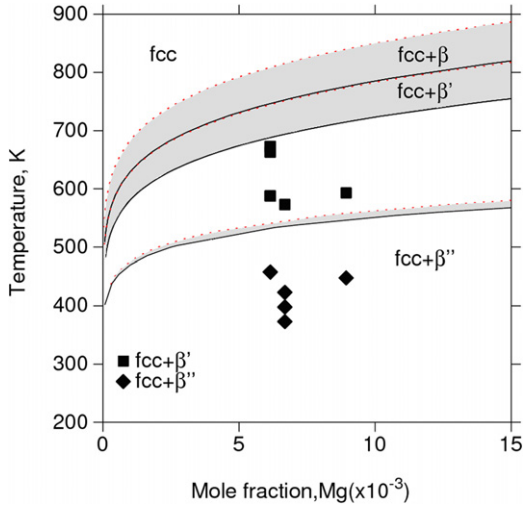

Fig. 5. Calculated solvus boundaries in the isopleth of 0.76 at.% Si with (■) fcc + β' phase region [1,3,59,61]; (♦) fcc + β'' phase region [1,60–62]; and the solvus of fcc/β from COST507 [9]. The solid lines indicate the solvus using first-principles enthalpies of formation and entropies for three precipitates. The dashed lines represent the solvus using modified enthalpic and entropic parameters. The width of the bands indicates the uncertainty in the solvus.

of Mg, the data are not considered to be accurate. The degree of agreement between the two phase boundaries is represented by the relative deviation in calculated temperatures, $\sqrt{\frac{\sum_i[(C_i-B_i)/B_i]^2}{N}}$ where C_i and B_i represent the two sets of data, and N the number of experimental data points. Given the fact that we have no adjustable or fitting parameters in the present calculations, we find the first-principles phase boundaries to be in very good agreement with COST507 database with the relative deviation of the solvus of fcc/β about 6.7%.

Even though the solvus boundary of β from first-principles is in reasonably good agreement with COST507, in order for us to make quantitative predictions of the metastable β' and β'' solvus boundaries, we wish to adjust our solvus curves slightly such that the calculated solvus of β agrees precisely with COST507. To achieve this, we apply correction parameters, k_H and k_S, which are the ratios between the enthalpies and entropies of formation for β-Mg_2Si phase from COST507 database and first-principles:

$$k_H = \frac{\Delta_f H^{Mg_2Si}_{COST507}}{\Delta_f H^{Mg_2Si}_{first-principles}} \tag{7}$$

$$k_S = \frac{\Delta_f S^{Mg_2Si}_{COST507}}{\Delta_f S^{Mg_2Si}_{first-principles}} \tag{8}$$

where $\Delta_f H^{Mg_2Si}_{COST507}$ and $\Delta_f H^{Mg_2Si}_{first-principles}$ correspond to enthalpy of formation of β-Mg_2Si phase from COST507 database and first-principles, respectively. The entropy of formation of β-Mg_2Si phase from COST507 database and first-principles are represented by $\Delta_f S^{Mg_2Si}_{COST507}$ and $\Delta_f S^{Mg_2Si}_{first-principles}$. The correction parameters are then applied to scale the values of $\Delta_f H^{Mg_{18}Si_{10}}_{first-principles}$, $\Delta_f H^{Mg_5Si_6}_{first-principles}$, $\Delta_f S^{Mg_{18}Si_{10}}_{first-principles}$ and $\Delta_f S^{Mg_5Si_6}_{first-principles}$ calculated from first-principles for β' and β'' phases. The modified enthalpic and entropic parameters for metastable phases can in turn be expressed as:

$$\Delta_f H^{Mg_aSi_b}_{modified} = k_H \times \Delta_f H^{Mg_aSi_b}_{first-principles} \tag{9}$$

$$\Delta_f S^{Mg_aSi_b}_{modified} = k_S \times \Delta_f S^{Mg_aSi_b}_{first-principles}. \tag{10}$$

The correction parameters and modified parameters for stable and metastable phase are shown in Table 4.

Fig. 5 shows the predicted phase boundaries of fcc/β, fcc/β' and fcc/β'' in the isopleth of 0.76 at.% Si from first-principles calculations. In this figure, the Gibbs energy function of the fcc phase is taken from Feufel et al. [9]. Using the first-principles enthalpies and entropies of formation of three precipitate phases, the solvus curves are predicted and shown as solid curves. Dashed lines indicate the predicted solvus curves by using the modified parameters as shown in Table 4. The width of the bands indicated the estimated uncertainty in the solvus curves. Even though the experimental solubility data is very scattered due to the transitory feature of the metastable phases, the measured stability ranges for β'-$Mg_{18}Si_{10}$ and β''-Mg_5Si_6 phases [1,3,59–62] are well captured in our predictions.

It should be pointed out that the above calculated phase boundaries represent the thermodynamic limits of phase equilibria, while the experimentally measured ones are affected by the interfaces between the fcc and precipitates. Typically, an interface changes from coherent, semi-coherent to incoherent due to the interplay between the interfacial energy and the strain energy associated with the size of precipitates. As the first precipitate formed during low-temperature aging, β'' has a coherent interface with the fcc matrix, while the interfaces of β' and β with the fcc matrix are semi-coherent and incoherent, respectively [63]. In our prior study, the coherent interfacial energy and strain energy of β'' were predicted to be around 100 mJ m^{-2} and 0.45 kJ/mole-atom, respectively [64]. The typical semi-coherent and incoherent interfacial energies are from 300– 1000 mJ m^{-2} [64,65], along with smaller strain energies because of the less deformation. As both interfacial and strain energies increase the Gibbs energy of precipitates, and hence result in increasing the solubility of (meta)stable phases in the fcc solution phase. Different experimental measurements of the metastable solvus reported in the literature might have been carried out at the different stages of the transitions, contributing to the significant scattering of phase boundary data.

4. Summary

Using first-principles calculations, we have computed the thermodynamic properties of (meta)stable precipitates in the Al–Mg–Si system. Along with the $T = 0$ K first-principles total energies, we use the frozen phonon approximation to calculate the enthalpies and entropies of formation of β-Mg_2Si, β'-$Mg_{18}Si_{10}$ and β''-Mg_5Si_6 phases. We find that the phonon contributions to

Table 4
Enthalpy and entropy of formation $\Delta_f H$ (kJ mol^{-1}) and $\Delta_f S$ (J mol^{-1}K^{-1}), respectively, in per mole of atom unit.

	First-principles calculations		Thermodynamic database [9]		Correction		Modified parameters	
	$\Delta_f H^a$	$\Delta_f S^a$	$\Delta_f H^b$	$\Delta_f S^b$	$\Delta_f H^b/\Delta_f H^a$	$\Delta_f S^b/\Delta_f S^a$	$\Delta_f H$	$\Delta_f S$
β-Mg_2Si	−17.7	−1.8	−21.74	−2.68	1.2265	1.490	−21.74	−2.68
β'-$Mg_{18}Si_{10}$	−12.6	0.2	N/A	N/A	N/A	N/A	−15.5	0.26
β''-Mg_5Si_6	3.5	4.5	N/A	N/A	N/A	N/A	4.3	6.7

$\Delta_f H^a$ enthalpy of formation from first-principles calculations.
$\Delta_f H^b$ enthalpy of formation from COST507 thermodynamic database.
$\Delta_f S^a$ entropy of formation from first-principles calculations.
$\Delta_f S^b$ entropy of formation from COST507 thermodynamic database.

Gibbs energies increase from β, β' to β'' and thus the bonding of Mg–Si weakens from β, β' to β''. The metastable β'' phase has the highest entropy and the weakest bonding among all the precipitates. The predicted enthalpy and entropy of formation for β-Mg_2Si at room temperature are in good agreement with the available experimental data. The Gibbs energies of formation of the precipitates from first-principles calculations are used to predict the solvus of metastable phases, and are in good agreement with the (admittedly scattered) experimental data from aging experiments.

Acknowledgements

This work was funded by the National Science Foundation (NSF) through Grant Grants Nos. DMR-0205232 and 0510180. First-principles calculations were carried out in part on the LION clusters at the Pennsylvania State University supported by NSF (Grant Nos. DMR-9983532, DMR-0122638, and DMR-0205232) and the Materials Simulation Center and the Graduate Education and Research Services at PSU, and in part on the resources of the National Energy Research Scientific Computing Center supported by the Office of Science of the US Department of Energy under Contract No. DE-AC03-76SF00098. C. Wolverton was supported by the US Automotive Materials Partnership (USAMP) through the US Council for Automotive Research (USCAR), contract 07-1876.

Appendix. Supplementary data

Supplementary data associated with this article can be found, in the online version, at doi:10.1016/j.calphad.2009.10.009.

References

[1] G.A. Edwards, K. Stiller, G.L. Dunlop, M.J. Couper, Acta Mater. 46 (1998) 3893–3904.
[2] L. Zhen, S.B. Kang, Mater. Sci. Technol. 14 (1998) 317–321.
[3] D.H. Bratland, O. Grong, H. Shercliff, O.R. Myhr, S. Tjotta, Acta Mater. 45 (1997) 1–22.
[4] I. Dutta, S.M. Allen, J. Mater. Sci. Lett. 10 (1991) 323–326.
[5] M. Takeda, F. Ohkubo, T. Shirai, K. Fukui, J. Mater. Sci. 33 (1998) 2385–2390.
[6] M. Murayama, K. Hono, M. Saga, M. Kikuchi, Mater. Sci. Eng. 250 (1998) 127–132.
[7] G. Kresse, J. Furthmuller, Phys. Rev. B 54 (1996) 11169–11186.
[8] G. Kresse, J. Furthmuller, Comput. Mater. Sci. 6 (1996) 15–50.
[9] H. Feufel, T. Godecke, H.L. Lukas, F. Sommer, J. Alloy. Compd. 247 (1997) 31–42.
[10] V. Ozolins, M. Asta, Phys. Rev. Lett. 86 (2001) 448–451.
[11] V. Ozolins, B. Sadigh, M. Asta, J. Phys.:Condes. Matter 17 (2005) 2197–2210.
[12] C. Ravi, C. Wolverton, V. Ozolins, Europhys. Lett. 73 (2006) 719–725.
[13] D. Vanderbilt, Phys. Rev. B 41 (1990) 7892–7895.
[14] J.P. Perdew, Y. Wang, Phys. Rev. B 45 (1992) 13244–13249.
[15] J.H. Chen, E. Costan, M.A. van Huis, Q. Xu, H.W. Zandbergen, Science 312 (2006) 416–419.
[16] P.M. Derlet, S.J. Andersen, C.D. Marioara, A. Froseth, J. Phys.:Condes. Matter 14 (2002) 4011–4024.
[17] D.W. Pashley, J.W. Rhodes, A. Sendorek, J. Inst. Met. 94 (1966) 41–49.
[18] M.H. Jacobs, Phil. Mag. 26 (1972) 1–13.
[19] H.J. Monkhorst, J.D. Pack, Phys. Rev. B. 13 (1976) 5188–5192.
[20] S.Y. Savrasov, Phys. Rev. B 54 (1996) 16470–16486.
[21] G.J. Ackland, M.C. Warren, S.J. Clark, J. Phys.:Condes. Matter 9 (1997) 7861–7872.
[22] F. Seitz, D. Turnbull, Solid State Physics, Academic Press, New York, 1964.
[23] P. Flubacher, A.J. Leadbetter, J.A. Morrison, Phil. Mag. 4 (1959) 273–292.
[24] K. Parlinski, J. Alloy. Compd. 328 (2001) 97–99.
[25] Y. Wang, Z.K. Liu, L.Q. Chen, Acta Mater. 52 (2004) 2665–2671.
[26] S. Baroni, S. de Gironcoli, A. Dal Corso, P. Giannozzi, Rev. Modern Phys. 73 (2001) 515–562.
[27] S. Shang, Y. Wang, R. Arroyave, Z.K. Liu, Phys. Rev. B. 75 (2007) 092101–092105.
[28] P.H. Dederichs, H. Schober, D.J. Sellmyer, in: K.H. Hellwege, J.L. Olsen (Eds.), Metals: Phonon States, Electron States and Fermi Surfaces, vol. 13a, Springer-Verlag, Berlin, 1981.
[29] R. Arroyave, Z.K. Liu, Phys. Rev. B 74 (2006) 174118–174133.
[30] E.F. Skelton, S.T. Lin, G.M. Rothberg, Acta Crystallogr. Sect. A A 30 (1974) 39–43.
[31] M. Blackman, Acta Crystallogr. 9 (1956) 734–737.
[32] A. van de Walle, M. Asta, G. Ceder, CALPHAD 26 (2002) 539–553.
[33] D.W. Shin, Z.K. Liu, CALPHAD 32 (2008) 74–81.
[34] A.T. Dinsdale, CALPHAD 15 (1991) 317–425.
[35] R. Pynn, G.L. Squires, Measurements of the normal-mode frequencies of magnesium, Proc. R. Soc. Lon., Ser. A. Math. Phys. Eng. Sci. (1972) 347–360.
[36] P.A. Temple, C.E. Hathaway, Phys. Rev. B 7 (1973) 3685–3697.
[37] J.D. Althoff, P.B. Allen, R.M. Wentzcovitch, J.A. Moriarty, Phys. Rev. B 48 (1993) 13253–13260.
[38] W. Yim, R. Paff, J. Appl. Phys. 45 (1974) 1456–1457.
[39] W.B. Whitten, P.L. Chung, G.C. Danielson, J. Phys. Chem. Solids 26 (1965) 49–56.
[40] C.J. Buchenau, M. Cardona, Phys. Rev. B 3 (1971) 2504–2507.
[41] D. McWilliams, D.W. Lynch, Phys. Rev. 130 (1963) 2248–2253.
[42] K. Parlinski, J. Lazewski, Y. Kawazoe, J. Phys. Chem. Solids 61 (2000) 87–90.
[43] J. Lazewski, K. Parlinski, W. Szuszkiewicz, B. Hennion, Phys. Rev. B 67 (2003) 094305–094313.
[44] S.L. Shang, Y. Wang, Z.K. Liu, Phys. Rev. B 75 (2007) 024302–024313.
[45] C. Ravi, C. Wolverton, Acta Mater. 52 (2004) 4213–4227.
[46] J.M. Eldridge, E. Miller, K.L. Komarek, Trans. AIME 239 (1967) 775–781.
[47] R. Geffken, E. Miller, Trans. AIME 242 (1968) 2323–2328.
[48] Y.K. Rao, G.R. Belton, Thermodynamic properties of Mg–Si system, in: N.A. Gokeen (Ed.), Chemical Metallurgy—A Tribute to Carl Wagner, The Metallurgical Society of AIME, 1981, pp. 75–96.
[49] S.J. Andersen, C.D. Marioara, R. Vissers, A. Froseth, H.W. Zandbergen, Mater. Sci. Eng. 444 (2007) 157–169.
[50] E.H. Dix, F. Keller, R.W. Graham, Trans. AIME 93 (1931) 404–420.
[51] H. Westlinning, W. Klemm, Z. Elektrochem. 49 (1943) 198–200.
[52] D. Hanson, M.L.V. Gayler, J. Inst. Met. 26 (1921) 321–355.
[53] K. Grjotheim, O. Herstand, S. Petrucci, R. Skarbo, J. Toguri, Rev. Rom. Chim. 7 (1962) 217–223.
[54] O. Kubaschewski, H. Villa, Z. Electrochem. 53 (1949) 32–40.
[55] G.M. Lukashenko, V.N. Eremenko, Zh. Neorg. Khim. 9 (1964) 2295–2296.
[56] H.J. Caulfield, Ph.D. Thesis, Iowa State University, quoted in [21], 1962.
[57] I. Brian, O. Knacke, Thermochemical Properties of Inorganic Substances, Springer-Verlag, New York, 1973.
[58] O. Kubaschewski, C.B. Alcock, Metallurgical Thermochemistry, Pergamon Press, New York, 1979.
[59] O.R. Myhr, O. Grong, H.G. Fjaer, C.D. Marioara, Acta Mater. 52 (2004) 4997–5008.
[60] C.D. Marioara, S.J. Andersen, J. Jansen, H.W. Zandbergen, Acta Mater. 49 (2001) 321–328.
[61] O.R. Myhr, O. Grong, S.J. Andersen, Acta Mater. 49 (2001) 65–75.
[62] C.D. Marioara, S.J. Andersen, J. Jansen, H.W. Zandbergen, Acta Mater. 51 (2003) 789–796.
[63] D.A. Porter, K.E. Easterling, Phase Transformations in Metals and Alloys, Chapman & Hall, London, 1992.
[64] Y. Wang, Z.K. Liu, L.Q. Chen, C. Wolverton, Acta Mater. 55 (2007) 5934–5947.
[65] Z.K. Liu, Acta Mater. 44 (1996) 3855–3867.